Two-Dimensional Condensing Vapor Flow on Parallel Flat Plates in an Enclosure

Yasunori Kobayashi* and Tsuyoshi Matsumoto†
University of Tsukuba, Sakura, Japan

A vapor flow of pure fluid condensing onto a vertical flat plate in an enclosure was examined in order to develop knowledge of the mechanism of vapor condensation and flowfield characteristics. A specific Pyrex glass thermosyphon-like container filled with a certain amount of pure fluid, with or without noncondensable gas, was heated and the upward vapor flow between a pair of cooled parallel plates installed in the upper portion of the container was investigated by means of temperature and pressure sensors as well as laser holographic interferometry. With a pure fluid only (single-component, two-phase flow) in the container, the entire flowfield of condensation region is uniform in density and temperature. On the other hand, with a pure fluid containing a noncondensable gas (two-component, two-phase flow), a distinct flowfield structure is obtained. Its characteristics are 1) the flowfield in the vapor/gas mixing region has a clear interfacial layer in the longitudinal or axial direction and a rather thick boundary layer near the cooled plate; 2) the condensing vapor flow has an oscillatory character with a low frequency of around 1 Hz, even in the steady-state flow and thermal conditions; and 3) a sharp pressure drop was observed at the initiation of nonequilibrium vapor condensation when a large temperature difference existed between the vapor and the cooled plates.

Introduction

A STUDY of thermofluid dynamics, including the phase change of fluid in an enclosure, has long been one of the central concerns in heat-transfer problems. However, a lack of understanding of the evaporation and condensation mechanism of fluids makes it difficult to formulate a sound model of the flowfield that can optimally design various heat-transfer devices such as heat exchangers, heat pipes, and other cooling systems. A recent development in heat pipe technology seems to expedite such basic studies as internal heat and mass transfer in the enclosure in order to maximize heat-transfer rates and to clarify the thermochemical action in the device. Although many efforts have been devoted to these subjects,[1-7] relatively few are concerned with the phenomena when a large temperature difference exists between the vapor and the solid surface and/or when noncondensable gas is present. Recent work on a kinetic approach[1,2] to the condensation/evaporation mechanism through the use of BGK model equations indicate a fine structure of the flowfield that classical theories[3,4] did not reveal. Numerical analyses of the internal flow in heat pipes and tubes[5-7] are also numerous, based on various assumptions and approximations. However, little experimental evidence is available to confirm these theories and analyses.

A fundamental and necessary first step in investigating these problems is a detailed flowfield survey and heat-transfer measurements in the upright enclosure conducted by means of conventional methods. Generally, it is understood that noncondensable gas in the thermosyphon occupies the upper portion of the condensation region during steady-state operation and that some finite vapor/gas mixing zone or interfacial layer separating the vapor flow from the noncondensable gas moves vertically according to the heat input rate. This behavior is similar to that acknowledged in the operation of variable conductance heat pipes (VCHP).[8,9] It is also known that the total heat-transfer rate of the thermosyphon drops drastically in the presence of a noncondensable gas.

Presented as Paper 85-1046 at the AIAA 20th Thermophysics Conference, Williamsburg, VA, June 19-21, 1985; received Aug. 5, 1985; revision received Aug. 8, 1986.

*Associate Professor, Institute of Engineering Mechanics. Member AIAA.

†Graduate Student, Graduate School in Engineering.

This paper presents some results of a detailed flowfield survey of a condensing vapor flow onto a cooled flat plate in the thermosyphon with emphasis on the effect of a noncondensable gas. The comparatively large fluctuations in temperature and pressure under steady-state flowfield and the sharp pressure variation at the initiation of vapor condensation onto the cooled plate are carefully investigated. Temperature and density distributions and mole fraction of the noncondensable gas in the interfacial layer are calculated from fringe patterns obtained by a real-time laser holographic interferometer together with the measured quantities.

Experimental Setup and Method

Thermosyphon Model

Figure 1 illustrates schematically two thermosyphon models used in this experiment. One (model A) is a simple Pyrex glass cylindrical tube of 50 mm i.d. and 300 mm in length used for extensive temperature and pressure measurements. In this model, three semiconductor-type pressure sensors are placed flush with the inner surface of the glass tube and 30 copper-constantan thermocouples are located at various places inside the tube. The other (model B) is a specially designed Pyrex glass tube of 50 mm i.d and 500 mm in length. The central portion of this tube (about 200 mm in length) is designed to have a square 45×45 mm cross-sectional area to make an optical window for visualization of the flowfield. These tubes are capped with the sealing flange, on the bottom side of which a pair of rectangular cooling panels (flat plates) are installed in parallel to realize a two-dimensional condensing vapor flow region in the model. These panels are about 25 mm wide, 150 mm long, and 1 mm thick, and are placed 14 mm apart facing each other at the test section of the tube. These plates are cooled by circulating water in a U-shaped, 6 mm o.d. cooling pipe placed behind the plates; an electric coil heater dipped in the working liquid at the bottom gives the liquid a heat energy to evaporate. In the model B, a pressure sensor and 10 thermocouples are installed so as not to disturb the path of a laser light flux for visualization. The pressure sensor of the latter is set at the top of the flange with 50 mm extension pipe, which is kept around 50°C by the heater in order to stabilize the output signal of the sensor measuring the surrounding temperature variations. In order to prevent vapor condensation, the optical window of the square test section is kept at about 60°C by applying a fine tungsten wire heater.

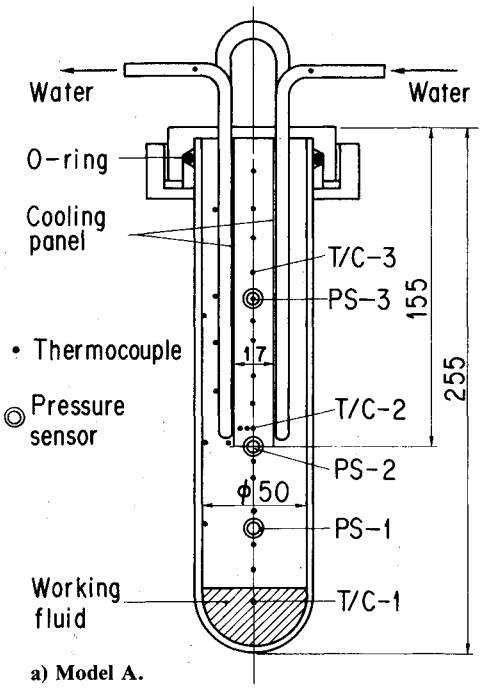

a) Model A.

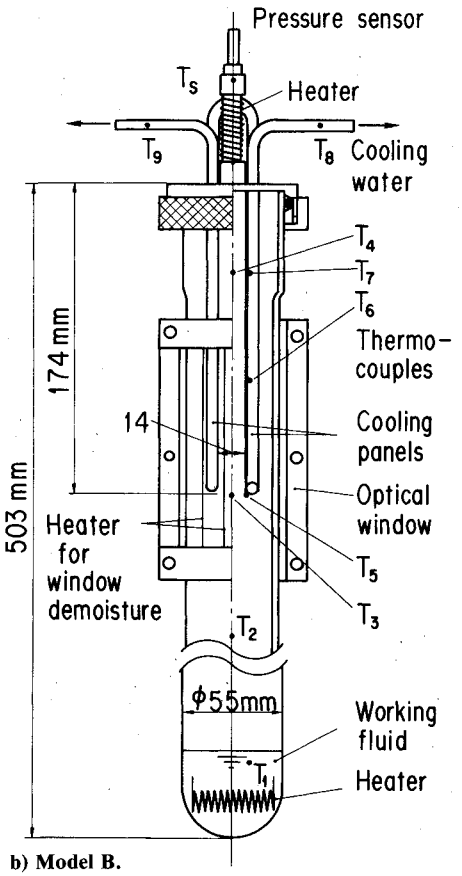

b) Model B.

Fig. 1 Thermosyphon-like enclosure models and their sensor locations (scale in mm).

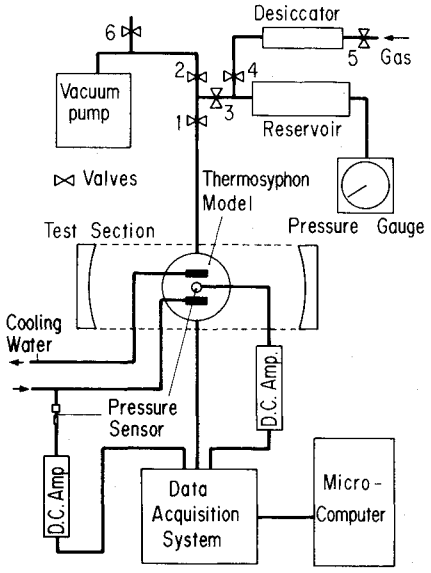

a) General view of setup.

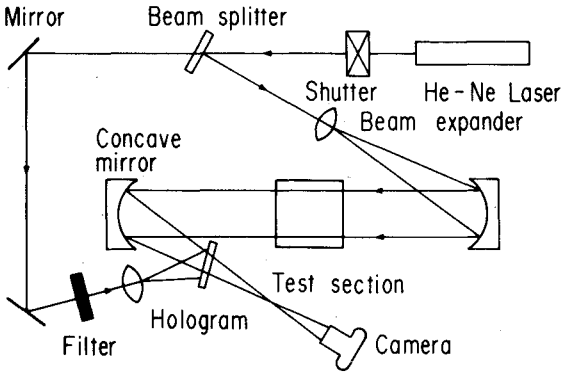

b) Laser holographic interferometer.

Fig. 2 Schematic of experimental setup and instrumentation.

Experimental Apparatus

The experimental setup and enclosure models used in the experiment are composed of the thermosyphon model, data acquisition system, and vacuum pump facility, as shown schematically in Fig. 2a. For flowfield visualization, the enclosure model (model B) is placed in the test section of the laser holographic interferometer (see Fig. 2b); the temperature and pressure variations at the time of visualization are measured in this configuration simultaneously. Extensive measurements of the temperature and pressure distributions in the flowfield are also conducted by using a different enclosure model (model A) that has almost the same vapor flowfield configuration as that of model B.

Laser Holographic Interferometer

Figure 2b shows an optical arrangement of the real-time laser holographic interferometer.[10,11] Distributions of the temperature, density, and mole fraction of a noncondensable gas in the vapor/gas mixing zone are obtained by analysis of the fringe pattern in the measured interferograms with the following assumptions: 1) the total pressure in the vessel is uniform and constant, 2) the noncondensable gas behaves as an ideal gas and the vapor is in a saturated condition corresponding to its temperature, 3) the vapor/gas interfacial layer has a finite thickness, and 4) the Gradstone-Dale relation formally holds in the vapor/gas mixture and its refractive index $\tilde{n}$ is expressed as,[12]

$$\tilde{n} = 1 + \bar{K} \cdot \tilde{\rho} \tag{1}$$

where $\tilde{\rho}$ is the density of the mixture and $\bar{K}$ a Gradstone-Dale constant of the mixture. The specific refractive index r of pure matter is defined by Lorenz and Lorentz as,

$$r = (n^2 - 1)/(n^2 + 2)/\rho \tag{2}$$

Since the specific refractive index is known to have a dominant nature when several materials are mixed in a manner such that they have weak molecular interactions with each other (i.e., gas mixtures), the following relation will approximately hold

for an n-component gas mixture:

$$\bar{r}=x_1r_1+x_2r_2+\ldots+x_nr_n \tag{3}$$

where $\bar{r}$ and x_i represent the specific refractive index and mass fractions of the components in the gas mixture, respectively. Therefore, the value of $\bar{K}$ in Eq. (1) can be obtained from Eq. (2) as,

$$K=x_1K_1+x_2K_2+\ldots+x_nK_n \tag{4}$$

with the use of the relations $\pi=rM$ and $K=(3\pi/2M)$, where π is the molecular refractive index and M the molecular weight of the pure material. In the present case of a vapor/gas two-component mixture, the averaged Gradstone-Dale constant is expressed concisely as,

$$\bar{K}=xK_g+(1-x)K_v \tag{5}$$

where x represents mass fraction of the noncondensable gas and g and v the noncondensable gas and vapor, respectively. With the prescribed assumptions, Eq. (5), and the aid of the equation of state for ideal gas and Dalton's rule of partial pressure of gas mixtures, distributions of the temperature, density, and mole fraction ω_g ($\omega_g=M\,x/\bar{M}$, where $\bar{M}$ is the molecular weight of the gas mixture) are numerically calculated provided that the total pressure of the flowfield is known from measurements.

Measurements and Data Acquisition

Simultaneous flowfield visualizations and steady-state temperature measurements were made with pure benzene as a working fluid and dried air and helium as a noncondensable gas. Impurities and foreign materials contained in the model are eliminated by alternate freezing (by vacuum pumping) and boiling (by heater) of the working fluid. A given amount of noncondensable gas was put into the thermosyphon model through a gas regulating reservoir. Interferograms and related temperature and pressure data were always taken after the thermal steady-state condition had been established in the model by changing the starting condition of the heat input and the partial pressure of the contained noncondensable gas. All the data and measurement information were stored in the microcomputer.

Extensive measurements of the temperature and pressure fluctuations of nonequilibrium thermal conditions having large temperature differences, as well as steady-state temperature distributions in the flowfield, were conducted in the following manner. Initially, the temperature and pressure variations were monitored by maintaining the model at a certain temperature level until thermal steady-state condition was established in the entire flowfield with no cooling water circulation (which is called an "uncooled" condition). The data acquisition was continued during and after a sudden circulation of cooling water in the panel (called a "cooled" condition) to investigate the occurrence of strong condensation caused by the large temperature difference produced between the vapor and panel at the initial moment of water circulation. Temperature and pressure changes with respect to the elapsed time were sampled every 0.1 s and stored in the microcomputer to be processed later off-line. Four kinds of pure liquids, viz., distilled water, benzene, acetone, and Freon 11 were examined in this experiment. Typical Reynolds numbers based on the vapor speed calculated from the measured heat-transfer rate and the gap distance between the cooling panels were of the order 50 for distilled water and 700 for benzene.

Results and Discussion

Figure 3 shows typical longitudinal or axial temperature distributions along the centerline of the flowfield in the "uncooled" and "cooled" steady-state thermal conditions obtained for distilled water and benzene with air as the noncondensable gas. The cooling panel is located in the axial direction between 0.4 and 1.0 in the nondimensionalized coordinate and the far left values in the individual curves express the evaporating liquid temperature in the container. These distributions indicate that the "cooled" vapor flowfield is not thermally uniform, but has a comparatively large temperature gradient. A temperature rise in the cooling panel toward its lower end indicates that the rate of vapor condensation is not uniform on the panel, but that a relatively large portion of the vapor condenses on the plate close to its lower end. This is because the noncondensable gas, which is confined in the upper region of the flowfield, covers the panel surface, thus

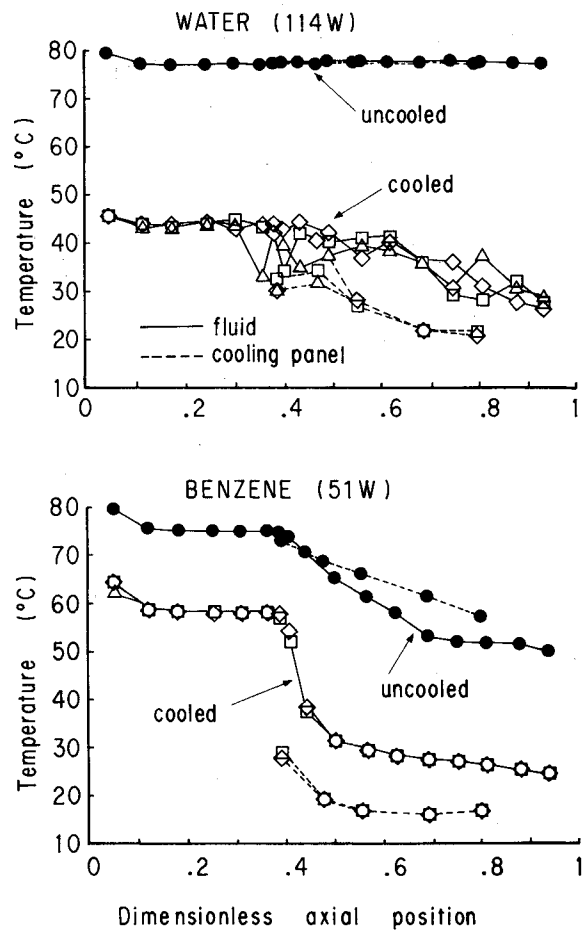

Fig. 3 Typical results of longitudinal temperature distributions obtained for distilled water and benzene.

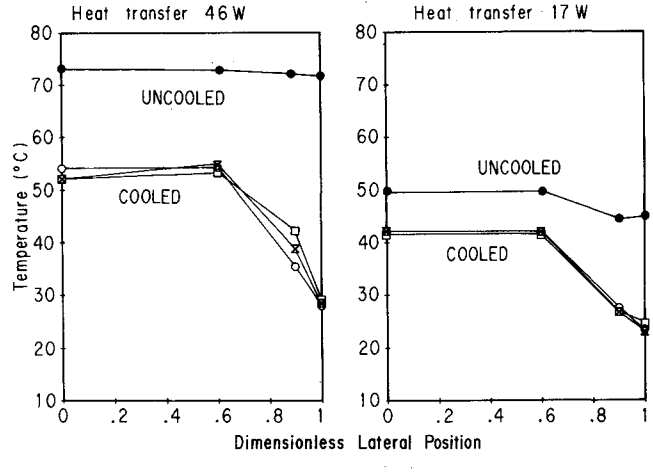

Fig. 4 Lateral temperature distributions at the lower end of the cooling panel.

preventing effective vapor condensation. A visual observation of the plate confirms the evidence that the upper portion of the panel is almost dry with little condensate, while the lower part is covered with liquid film flowing down and dripping into the evaporator section of the model. It is also apparent that the condensation region of distilled water generates unstable temperature fluctuations even in a steady-state thermal condition of the flowfield, while benzene condenses in a relatively stable manner with much smaller amplitude fluctuations. This apparent difference of condensation mode is caused by the evaporation of the fluid under investigation, which results from the differences in the thermal properties, especially surface tension, of the two fluids. A more detailed interpretation will be given below in the discussion of the temperature fluctuations in Figs. 5 and 6. A common feature of these "cooled" distributions is that relatively large temperature differences are maintained between the panel and vapor. Lateral temperature distributions of benzene perpendicular to the surface of cooling panel at its lower end are shown in Fig. 4. The origin of the abscissa corresponds to the centerline of the flowfield and unity to the surface of cooling panel. This figure implies the existence of a relatively thick thermal boundary layer on the panel surface and the temperature difference across it becomes large with the increasing heat-transfer rate.

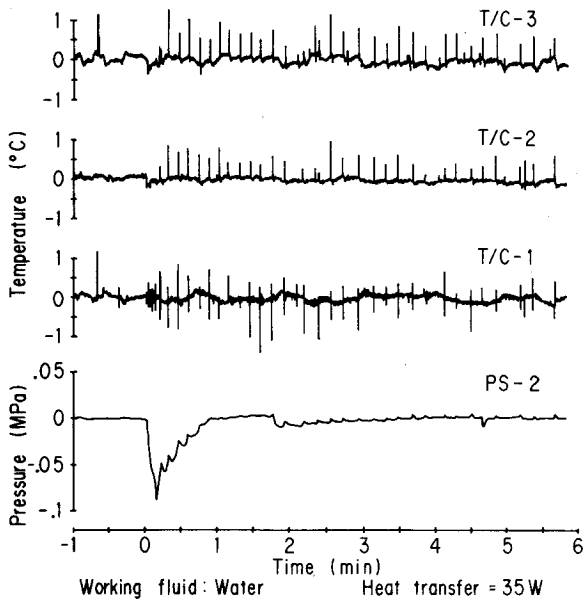

Fig. 5 Temperature fluctuations and pressure changes when and after the panel is cooled.

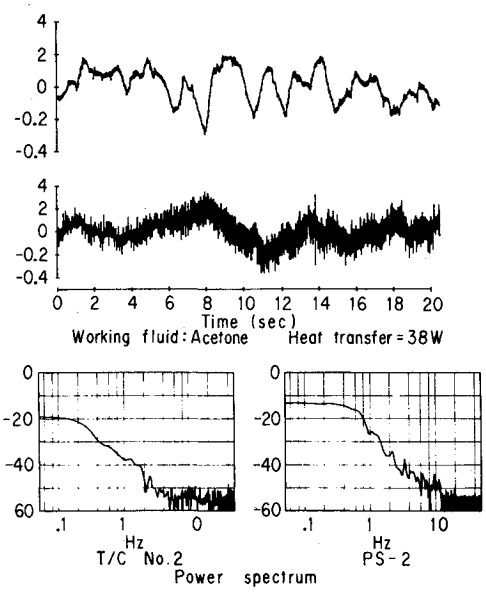

Fig. 6 Typical vapor temperature and pressure variations and power spectrums of acetone fluid.

In Fig. 5, the top curve shows the temperature fluctuations (the ac component of the output voltage signals detected by the thermocouples) obtained at three different locations in the model (A in Fig. 2) for distilled water before and after the panel is cooled. Cooling water starts to circulate at the moment corresponding to time = 0 in the abscissa. One can see that the large negative pulses detected in the liquid (T/C 1 in Fig. 5) is in synchronization with that of the positive pulses in the vapor (T/C 2 and 3). It can be interpreted that a burst of strong boiling removes a large amount of heat energy from the liquid, causing an instantaneous temperature drop in contrast to a temperature rise in the vapor. Close visual observation confirms the intermittent burst of large bubbles in the liquid water in the evaporator section at just the moment strong spikes appear on the recorder. Similar resulting fluctuations are also shown in Fig. 6 for acetone, but the fluctuation mode is quite different from that in Fig. 5. Thus, the heat input rate as well as the working fluid used affected the pulsative behaviors observed in the enclosure model, especially their strength and frequency. The differences in the physical properties of the various working fluids utilized, such as latent heat, surface tension, viscosity, thermal conductivity, etc., appear to generate the different fluctuation modes. Within the scope of this experiment, temperature fluctuations were always observed in the steady-state condensing vapor flow; distilled water produced the most pronounced fluctuations and benzene and Freon 11 the least. This phenomenon is basic in the behavior of fluid in an enclosure containing both condensation and evaporation sections and is enhanced by the "cooled" condition in which a large temperature difference is maintained between the vapor and the plate.

A time history of the pressure changes in the vapor flow is shown in the bottom curve in Fig. 5. These data indicate that an unusually large pressure drop appears at the initiation of the cooling water and that the pressure gradually returns to the steady-state condition. This transient phenomenon was also consistently observed at the moment of changing from "uncooled" to "cooled" conditions and thus was not considered as a detecting error in the pressure sensor. A similar pressure change was detected with a Bourdon's tube, which, unlike semiconductor-type sensors, does not have a temperature-sensitive element to measure pressure. One possible explanation of the pressure drop might be that the large temperature difference created between the panels and the vapor at the initiation of cooling water will generate a strong and sudden vapor condensation on the plate, reducing the vapor density instantaneously like a rarefaction wave. The small spikes superposed on this pressure curve correspond to pulses in the temperature fluctuations which implies an intimate correlation between pressure and temperature through the phase change of the working fluid in the container.

Typical power spectrums of the temperature and pressure fluctuations observed in the steady-state condensation region of acetone fluid are shown in Fig. 6. This figure indicates that the temperature and pressure distributions have similar spectrums, with maximum power at a frequency level in the range of 1 Hz. This similarity again confirms the close correlation between temperature and pressure that is characteristic of vapor flows experiencing phase changes in an enclosure.

Figure 7 shows the heat-transfer performance with respect to vapor flow velocity realized in model A with partial pressure P_g of the noncondensable gas as a parameter. The nondimensional heat-transfer rate or Nusselt number Nu is defined as,

$$Nu = \ell h/k = \ell Q_i/kS\Delta T$$

where ℓ is a gap distance between the panels, Q_i a measured value of heat input, ΔT the temperature difference between the vapor and the panel, S the surface area of two flat plates, and k the thermal conductivity of the vapor. The Reynolds number Re is estimated by using ℓ and the mean velocity of the vapor flow calculated from Q_i, under the assumption that all of the heat input is converted to the evaporating working liquid. Therefore, the vapor flow velocities obtained in the experiment are proportional to the heat input and are in the range of 0.02–0.70 m/s. Figure 7 shows a commonly acknowledged feature, i.e., Nusselt numbers without noncondensable gas are relatively large, whereas those with noncondensable gas are small, particularly when the Re or heat input rate is small. In other words, the existence of noncondensable gas reduces the heat-transfer rate, an adverse effect that becomes eminent with the increasing amount of noncondensable gas. This is again because the noncondensable gas prevents effective vapor condensation on the plate, playing the same role as the gas in a variable conductance heat pipe (VCHP). When its velocity is increased for Re beyond 1000, the vapor flow becomes turbulent and the heat-transfer mechanism may change from diffusion dominant to convection dominant, which will augment the heat-transfer rate as shown in Fig. 7. Presently, no appreciable interpretation is given for an Nu distribution of a pure fluid having a peak value at around $Re = 100$. This problem is still under reinvestigation, but one possible cause may be that the growth in the thickness of the liquid film on the plate retards the vapor condensation rate.

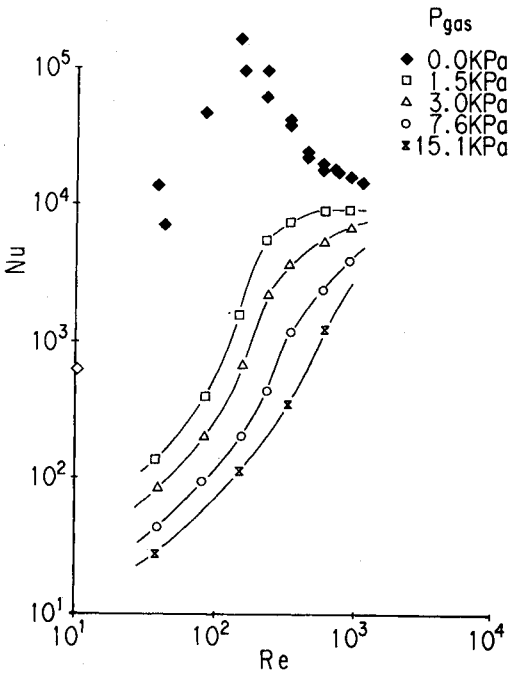

Fig. 7 Heat-transfer rates and vapor flow velocity of benzene fluid.

Figure 8 shows some typical density distributions of the vapor/gas interface layer in the steady-state condensation region visualized by the interferometer. These photographs show the density contour fringe patterns of the interface between benzene (the working fluid) and helium (the noncondensable gas) in the region about one-third above the lower edge of the cooling panel. It is observed that there exists a broad interfacial layer 20–30 mm thick, indicating a large axial density gradient and that it shifts upward as the heat input rate is increased. These curved spatial fringe distributions also indicate the existence of a boundary layer in the vicinity of the cooling panel, which may be called a "condensation layer" because of its large density gradient.

A typical quantitative result of distributions of the temperature, density, and mole fraction of the noncondensable gas obtained from the interferogram of Fig. 8b is shown in Fig. 9. The calculation is made by assuming that the mole fraction at the outermost end of the fringes (numbered 39 in Fig. 9) equals zero. Estimated errors involved in this analytical method are on the order of 2–3°C in terms of temperature. The heat input rate Q_i is calculated from the electrical power applied to the heater. Figure 10 shows the same distributions as that of Fig. 9 expressed in the form of graphs along the flowfield centerline across the interfacial layer of the vapor in the case of two types of noncondensable gases (helium and dried air). The mole number of the contained gas is 0.04 and the heat input rate is 77 W for both cases. Zero in the abscissa represents the position of lower end of the cooling panel. It should be noted that the interfacial layer for helium is about 1.5 times thicker than that for air, probably due to larger binary mass diffusivity of helium. In addition, comparatively large discrepancy in density profiles for helium and air will be created by the difference in their molecular weight. Relatively sharp gradients in the temperature and density profiles are due to the convective effect of the upward vapor flows superimposed on the diffusion of the gas. The important information shown in Fig. 10c is that the interfacial layer will clearly

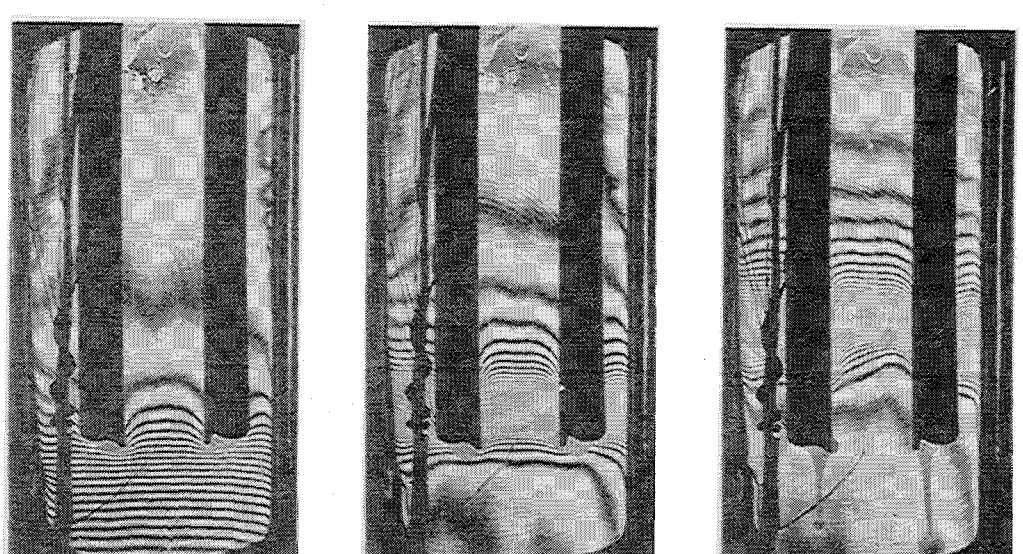

a) Heat input rate 19.2 W. b) Heat input rate 76.7 W. c) Heat input rate 235.0 W.

Fig. 8 Movement of vapor/gas interfacial layer visualized in the condensation region.

Qi : 76.7 W
Gas :He 100 ml
(1atm,20°C)

P : 39.2 KPa
T1 : 53.7°C
T2 : 58.2°C
T3 : 53.3°C
T4 : 11.9°C
T5 : 19.6°C
T6 : 11.1°C
T7 : 10.7°C

No.	T(°C)	ρ(Kg/m³)	ω_g	No.	T(°C)	ρ(Kg/m³)	ω_g
1	6.1	0.234	0.878	21	43.2	0.856	0.326
2	11.5	0.282	0.838	22	44.0	0.878	0.305
3	15.7	0.326	0.801	23	44.7	0.900	0.285
4	19.1	0.367	0.766	24	45.4	0.921	0.265
5	21.9	0.406	0.732	25	46.1	0.942	0.246
6	24.3	0.443	0.700	26	46.7	0.963	0.227
7	26.5	0.478	0.669	27	47.3	0.983	0.208
8	28.4	0.511	0.640	28	47.9	1.003	0.189
9	30.1	0.543	0.612	29	48.5	1.022	0.171
10	31.6	0.574	0.584	30	49.1	1.042	0.153
11	33.1	0.603	0.558	31	49.6	1.060	0.135
12	34.4	0.632	0.532	32	50.1	1.079	0.117
13	35.6	0.660	0.507	33	50.7	1.098	0.100
14	36.8	0.686	0.482	34	51.2	1.116	0.083
15	37.9	0.713	0.458	35	51.6	1.134	0.066
16	38.9	0.738	0.435	36	52.1	1.151	0.049
17	39.8	0.763	0.412	37	52.6	1.169	0.033
18	40.7	0.787	0.390	38	53.0	1.186	0.016
19	41.6	0.811	0.368	39	53.5	1.203	0.000
20	42.4	0.834	0.347				

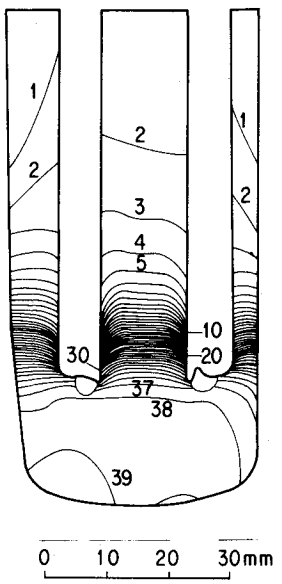

Fig. 9 Distribution of temperature, density, and mole fraction calculated from interferogram of Fig. 8b.

separate the pure vapor region from the noncondensable gas one, but that the latter actually contains a certain amount of vapor equaling the saturated thermal condition corresponding to a temperature of the gas region. Figure 11 shows another profile calculated for the temperature and mole fraction of the same flow condition in the flowfield perpendicular to the cooling panel at the location indicated by the arrows in Figs. 10a and 10c. The X symbol indicates the lateral distance from the centerline of the flowfield and Y the longitudinal position measured from the lower edge of the cooling panel. A mole fraction of the noncondensable gas becomes large near the surface because of the decreasing partial pressure of the condensing vapor toward the surface of the cooled plate and the relatively dense gas layer is formed.

The fringe patterns stayed stable and clear only when the heat input was small (up to a maximum of 250 W in this experiment). When the larger heat input was applied, the whole vapor flowfield becomes unstable and the strong convective effect of vapor flow distorted the stable fringe pattern of interfacial layer greatly (see, for example, Fig. 8c), finally extinguishing the whole fringe patterns. It should also be noted that the assumptions used for analyzing the fringe patterns are valid only when the convective mixing remains small in the flowfield.

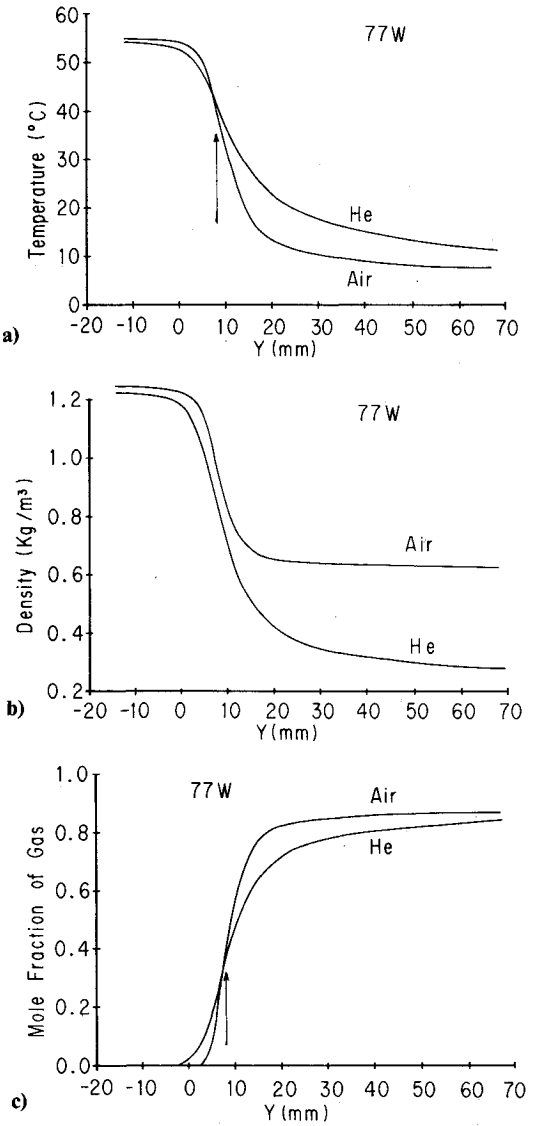

Fig. 10 Distributions of temperature, density, and mole fraction along the longitudinal flow direction.

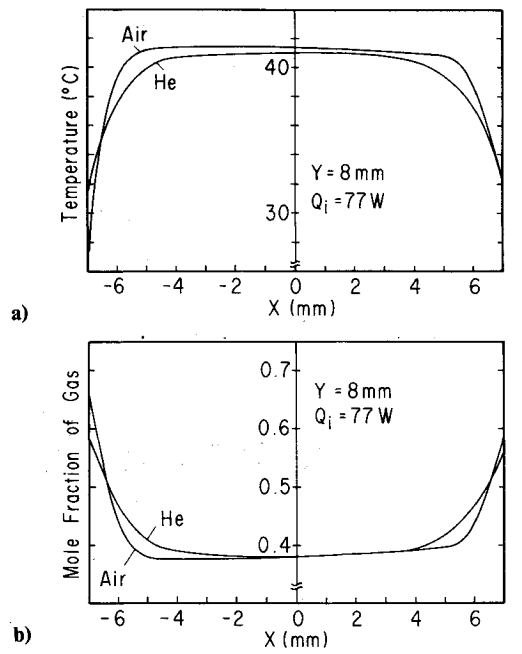

Fig. 11 Distributions of temperature and mole fraction along the lateral flow direction.

Conclusions

1) The entire flowfield of pure vapor is uniform and virtually no temperature differences are observed between the vapor and the cooled panel. On the other hand, when noncondensable gas is contained, a gas/vapor interfacial layer appears, clearly indicating the separation of gas from vapor regions, although the gas region contains the saturated vapor corresponding to the temperature of that region.

2) The interfacial layer has a two-dimensional structure of large longitudinal and lateral density gradients, a structure particularly prominent when the temperature differences are kept large between the vapor and the cooled surface. The density gradient in lateral directions may be called a "condensation layer."

3) Temperature and pressure fluctuations of the flowfield vary greatly both for unsteady and steady thermal conditions and are closely related to the thermal condition of the working liquid inside the container, especially to the boiling phenomena of the liquid.

4) The adverse effect of noncondensable gas on the heat-transfer rate in the enclosure is quite evident in the case of low heat input, an effect that becomes larger with the increase of a noncondensable gas. This effect is closely related to the variation of effective surface area of the cooled plate for vapor condensation, which is primarily determined by the location of the vapor/gas interfacial layer.

5) A sharp pressure drop appears at the moment of transition from the initial "uncooled" to the "cooled" condition. The pressure gradually recovers to the steady pressure level corresponding to the saturated thermal condition in the enclosure. This transient phenomenon of the pressure drop is probably due to the rarefaction effect generated by a strong vapor condensation on the plates, but the detailed mechanism of this phenomenon has not yet been clarified.

References

[1]Onishi, Y., "A Two-Surface Problem of Evaporation and Condensation in a Vapor-Gas Mixture," *Proceedings of 14th International Symposium on Rarefied Gas Dynamics*, 1984, pp. 875–884.

[2]Aoki, K., "Kinetic Theory of Unsteady Evaporation and Condensation Caused by Sudden Change of Wall Temperature," *Proceedings of 14th International Symposium on Rarefied Gas Dynamics*, 1984, pp. 885–892.

[3]Sparrow, E. M. and Lin, S. H., "Condensation Heat Transfer in the Presence of a Noncondensable Gas," *Transactions of ASME*, Ser. C, Vol. 86, 1964, pp. 430–436.

[4]Rose, J. W., "Condensation of a Vapor in the Presence of a Non-Condensing Gas," *International Journal of Heat and Mass Transfer*, Vol. 12, 1969, pp. 233–237.

[5]Simoji, S., Kimura, H., and Matsushita, T., "Prediction of Evaporator Temperature of a Gas Loaded Heat Pipe by the Diffusion Front Model," *Proceedings of 3rd International Heat Pipe Conference*, 1978, pp. 155–161.

[6]Busse, C. A. and Prenger, F. C., "Numerical Analysis of Vapor Flow in Cylindrical Heat Pipes," *Proceedings of 5th International Heat Pipe Conference*, Pt. 1, 1984, pp. 214–219.

[7]Spendel, Th., "Laminar Film Condensation Heat Transfer in Closed Two-Phase Thermosyphon," *Proceedings of 5th International Heat Pipe Conference*, Pt. 1, 1984, pp. 208–213.

[8]Dunn, P. D. and Reay, D. A., *Heat Pipes*, 2nd ed., Pergamon Press, Oxford, England, 1978, pp. 218–254.

[9]Tien, C. L. and Chen, S. J., "Non-Condensable Gases in Heat Pipes," *Proceedings of 5th International Heat Pipe Conference*, Pt. 1, 1984, pp. 97–101.

[10]Trolinger, J. D. and O'Hare, J. E., "Aerodynamic Holography," AEDC-TR-70-44, 1970.

[11]Kobayashi, Y., Kaneko, M. and Matsumoto, T., "Flow Field Visualization of Vapor Condensation in the Enclosure," *The Institute of Space and Astronautical Science Report*, SP. 1, 1983, pp. 241–245.

[12]Emrich, R. J. (ed.), *Methods of Experimental Physics*, Academic Press, New York, Vol. 18, Pt. A, 1981, pp. 346–356.